

This is the **accepted version** of the journal article:

Otaegui, Jaume Ramon; Ruiz-Molina, Daniel; Latterini, Loredana; [et al.].
«Thermoresponsive multicolor-emissive materials based on solid lipid nanoparticles». *Materials Horizons*, Vol. 8, Issue 11 (November 2021), p. 3043-3054. DOI 10.1039/d1mh01050f

This version is available at <https://ddd.uab.cat/record/266072>

under the terms of the  **CC BY** COPYRIGHT license

Thermoresponsive Multicolor-Emissive Materials Based on Solid Lipid Nanoparticles

Jaume Ramon Otaegui, Daniel Ruiz-Molina, Loredana Latterini, Jordi Hernando and Claudio Roscini**

J. R. Otaegui, Prof. D. Ruiz-Molina, Dr. C. Roscini
Catalan Institute of Nanoscience and Nanotechnology (ICN2), CSIC and BIST, Campus UAB,
Bellaterra, 08193 Barcelona, Spain
E-mail: claudio.roscini@icn2.cat

J. R. Otaegui, Dr. J. Hernando
Departament de Química, Universitat Autònoma de Barcelona, Edifici C/n, Campus UAB,
08193 Cerdanyola del Vallès, Spain
E-mail: jordi.hernando@uab.cat

Prof. L. Latterini
Department of Chemistry, Biology and Biotechnology, Perugia University, Via Elce di sotto,
8, 06123 Perugia, Italy

Keywords: thermofluorochromism, phase change materials, solid lipid nanoparticles, multicolor emission, smart materials

Abstract: Despite the recent advances in the field of thermofluorochromism, the fabrication of thermoresponsive multicolor-emissive materials in a simple, low-cost and versatile manner still remains a challenge. Herein we accomplish this goal by expanding the concept of matrix-induced thermofluorochromism, where a sudden two-state variation of dyes' emission is promoted by the solid-liquid transition of a surrounding phase change material (e.g., paraffins). We demonstrate that this behavior can be transferred to the nanoscale by the synthesis of dye-loaded solid lipid nanoparticles, different of which can then be combined into a single platform to obtain multicolor thermofluorochromism using a single type of emitter. Because of the reduced dimensions of these particles, they can be utilized to prepare transparent nanocomposites and inkjet-printed patterns showing complex thermoresponsive luminescent signals and applications ranging from smart displays to thermal sensing and high-security anti-counterfeiting.

Introduction

Thermally-responsive luminescent materials are gaining increasing attention because of their dual function as high-performance temperature indicators¹⁻⁴ and stimuli-sensitive components in smart functional devices.⁵⁻⁹ Of special interest in this area is to accomplish thermally-tunable multicolor emission - i.e., multicolor thermofluorochromism, which can be exploited in a variety of applications ranging from wide range temperature sensing^{1,3,4,10-15} to high-security anti-counterfeiting,^{8,9,16-18} white light generation¹⁹⁻²¹ and smart displays.⁷ Several methodologies have already been reported for the development of thermoresponsive multicolor luminescent systems,²² which can be essentially grouped in two categories: (a) the synthesis of emitters intrinsically responding to temperature (e.g., nanoparticles^{12,15}, molecular chromophores^{13,14,16,19,20,23-26}); and (b) the use of thermally-sensitive matrices that modulate the luminescence of the incorporated fluorophores (e.g., polymers,^{7,10,11,17,27} gels,²⁸⁻³⁰ liquid crystals^{31,32}). However, for translation into the market, further efforts are required to derive multicolor thermofluorochromic materials that are cost-effective, easily scalable and integrable into devices, extremely robust and highly tunable both in emission color and switching temperature range.

In this work we hypothesize that all these challenges can be faced at once with the miniaturization of thermally-sensitive matrices. For this we have chosen fully commercially available and low-cost organic phase change materials (PCMs, e.g., fatty acids, paraffins), which have already been shown by us³³⁻³⁵ and others³⁶⁻⁴⁰ to promote reversible fluorescence changes of dispersed molecular emitters upon solid-liquid transition (**Figure 1a**). Despite its multiple advantages for the preparation of thermofluorochromic materials, the use of bulk dye-PCM mixtures unfortunately hampers the realization of thermally-tunable multicolor emission, as they only exhibit an abrupt two-color luminescence switch around the melting point of the matrix. Consequently, variation of either the emitter of choice or of the composition of a dye mixture is required to obtain a different color switching behavior.^{33-36,40} To overcome this

limitation, we propose herein to structure emitter-PCM mixtures into nanometer-sized particles melting at different temperatures. By combining several of these nanoparticles in a single platform, their emission switching should take place sequentially at distinct temperatures and, as a result, intermediate fluorescence colors should be generated (Figure 1b-c).

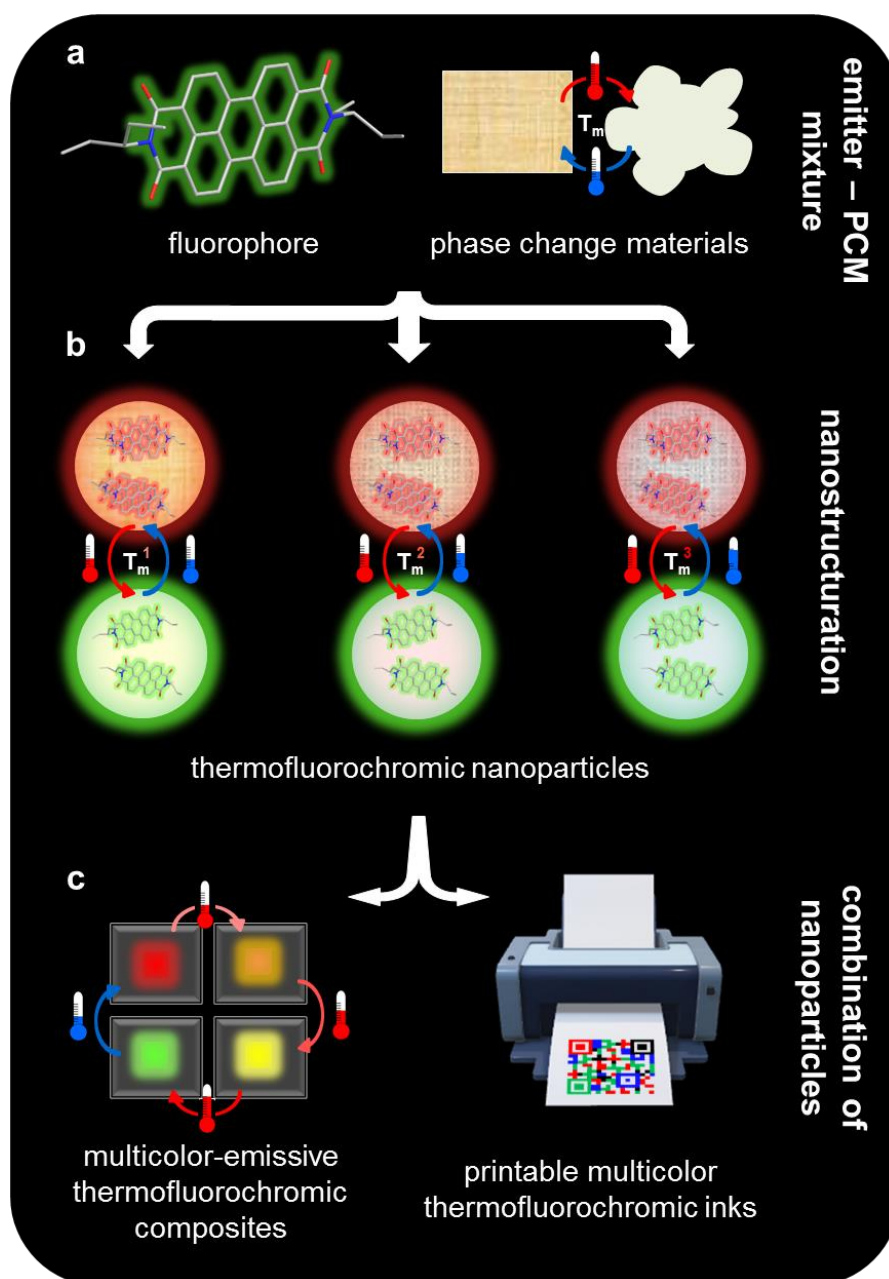


Figure 1. Strategy devised in this work to achieve multicolor thermofluorochromism by a) combining commercially-available fluorophores and phase change materials, b) miniaturizing these mixtures into nanoparticles, and c) integrating several different of the resulting nanostructures in a single platform, which allows the preparation of multicolor-emissive thermally-responsive composites and printable inks using just one type of emitter.

Several advantages should result from our approach towards multicolor thermofluorochromic materials. First, multicolor emission could be achieved with only one type of emitter, a very much desired property to reduce the cost and complexity of the final system^{20,24} that herein would enable straightforward fabrication from a reduced number of commercially available ingredients. Importantly, these appealing features would not come at the expense of the versatility of the resulting materials, whose thermal response should be easily tuned by varying the melting temperatures of the PCMs involved. In addition, miniaturization of the thermofluorochromic dye-PCM mixtures down to the nanoscale must facilitate their incorporation into functional devices (Figure 1c). Thus, because of their small sizes, dye-PCM nanostructures could be dispersed in supporting matrices to prepare composite layers exhibiting high light transparency, an increasingly demanded attribute for instance in smart luminescent displays⁴¹ and solar concentrators.^{31,42} Furthermore, stable water-based colloidal inks could be prepared that comply with the tight limitations imposed by the reduced nozzle dimensions in inkjet printing, which is the preferred technique for the deposition of well-defined stimuli-sensitive luminescent patterns for a number of purposes (e.g., in anti-counterfeiting^{9,43}).

Results and Discussion

Nanostructuration of thermofluorochromic materials

To prove our concept for the preparation of multicolor thermofluorochromic materials, we have chosen *N,N'*-bis(1-hexylheptyl)perylene-3,4,9,10-bis(dicarboximide), a highly stable and bright perylendiimide (PDI, Figure S1a) fluorophore that can be commercially purchased or readily synthesized.^{44,45} Although PDI has not been used yet for the realization of PCM-induced thermofluorochromism, it presents several crucial properties to enable this type of behavior. Because of the branched side alkyl chains introduced at the *N*-imide positions, PDI presents good solubility in organic liquid solutions, where it normally shows very high

quantum yield green fluorescence ($\lambda_{em}^{max} \sim 535$ nm, $\Phi_{em} \sim 1$ in most solvents). However, its polyaromatic core favors π - π supramolecular interactions at large concentrations or in poor solvents, which often results in red-shifted excimer-like emission ($\lambda_{em}^{max} \sim 650$ nm) due to self-aggregation. For instance, this is the case of solid supramolecular structures^{44,45} or highly-loaded polymer nanoparticles, where rather strong excimer-type emission is observed thanks to the presence of the swallow alkyl tails that limit the extent of self-quenching by formation of poorly fluorescent, tightly bound π -stacks. Accordingly, we expect the solubility of PDI and, as a result, its emission to dramatically vary upon liquid-to-solid transition of the surrounding PCM matrix, as already described for other organic fluorophores;^{33-35,37,40} i.e., the dye molecules should pass from being homogeneously dissolved in the liquid PCM as monomeric-emitting species to form excimer-emitting aggregates in the solid PCM. Actually, when dissolved at appropriate concentrations ($c_{PDI} \sim 0.1 - 0.2$ wt%) in simple paraffinic PCMs such as eicosane (EC, $T_m = 36.5$ °C⁴⁶) or octacosane (OC, $T_m = 61.3$ °C for OC⁴⁶), we found that selective PDI aggregation takes place upon crystallization of the surrounding matrix, as proven by the broad and unstructured UV-vis absorption spectrum measured (Figure S1b). Consequently, red excimer-like emission was observed in the bulk solid state of PDI-paraffin mixtures, while melting led to PDI disaggregation and redissolution in the liquid PCM that in turn caused a sharp, reversible and repeatable emission change to lime green monomeric fluorescence (**Figure 2a** and Figure S1c).

Prompted by these results, we next explored the nanostructuration of PDI-based thermofluorochromic materials. In particular, we focused our attention on the preparation of solid lipid nanoparticles (SLPs)⁴⁷ that preserve the thermoresponsive behavior of the PDI-PCM mixtures investigated in bulk. To illustrate this concept, we synthesized PDI-loaded OC SLPs ($c_{PDI} = 0.22$ wt%, PDI@OC_SLPs) by homogenizing through ultrasonication a melted mixture of these compounds in an aqueous solution of poly(vinyl alcohol) (PVA) and successively cooling down the resulting nanoemulsion by fast addition of cold water (see SI

for more details). TEM measurements confirmed the successful formation of SLPs (91 ± 44 nm, Figure 2b), which at room temperature preserved the characteristic aggregation-induced red excimer-like emission observed in the solid bulk mixture (Figure 2c).

Thanks to their PVA stabilizer layer, PDI@OC_SLPs showed good colloidal stability and retained their structural integrity when the resulting aqueous suspension was heated above OC melting point (e.g., 70 °C). Interestingly, a reversible fluorescence switch from red to lime green was concomitantly observed - i.e., from excimer-like to monomeric PDI luminescence-, thus demonstrating that PDI-loaded PCMs preserve the temperature emission modulation of the bulk material (Figure 2d and Figure S2a). This behavior was also encountered for PDI-loaded SLPs made from other paraffins with different melting points, such as EC ($c_{\text{PDI}} = 0.22$ wt%, PDI@EC_SLPs, $T_m = 36.5$ °C⁴⁶) and tetracosane ($c_{\text{PDI}} = 0.22$ wt%, PDI@TC_SLPs, $T_m = 50.3$ °C for TC⁴⁶). As a result, red-to-green switchable fluorescent nanoparticles could be prepared that vary their optical properties at distinct temperatures (Figure 2e and Figure S2b), which is one of the requirements for our strategy toward multicolor thermofluorochromism.

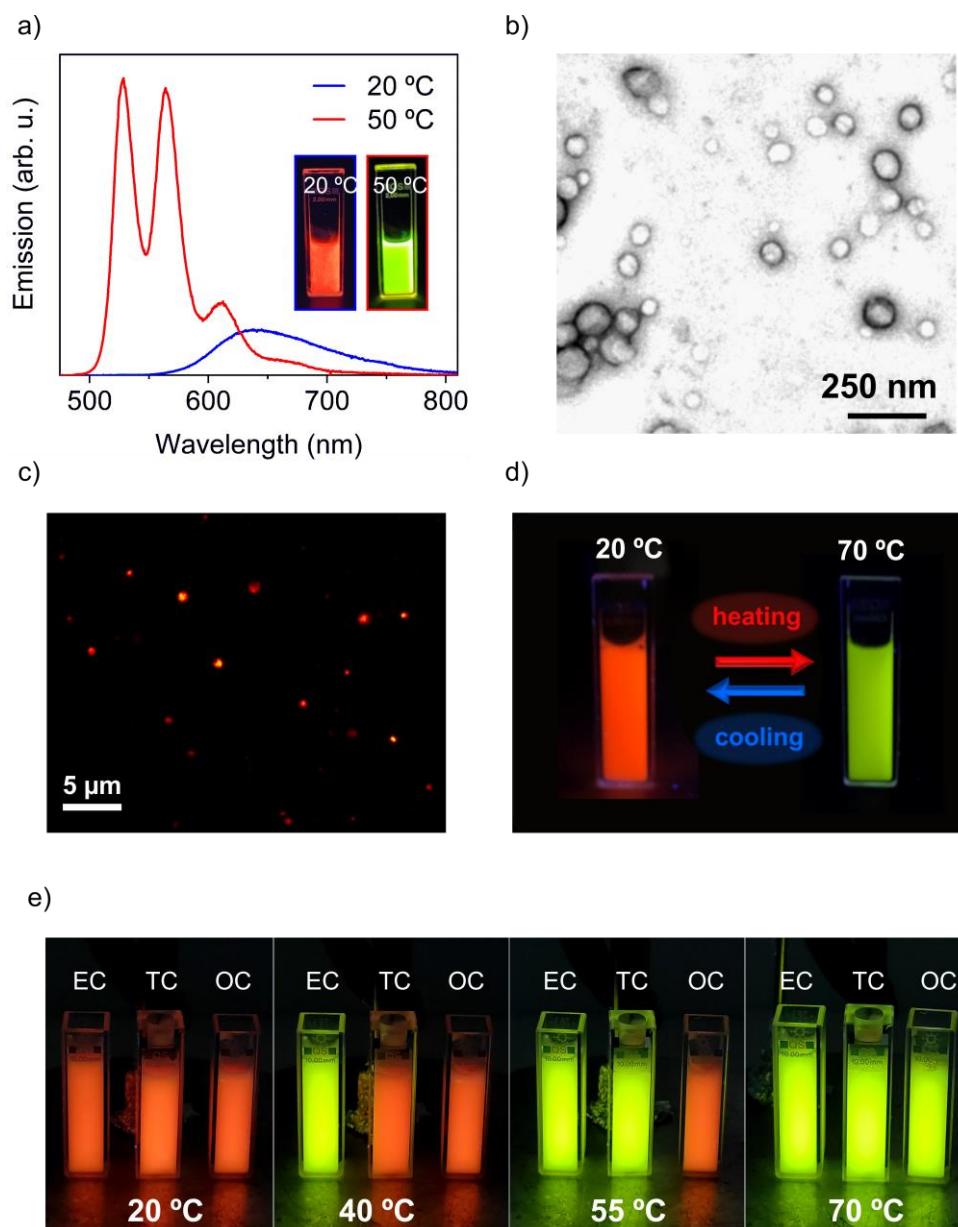


Figure 2. a) Variation of PDI emission spectrum ($\lambda_{\text{exc}} = 445 \text{ nm}$) in bulk solid ($T = 20 \text{ }^\circ\text{C}$) and melted ($T = 50 \text{ }^\circ\text{C}$) EC solutions ($c_{\text{PDI}} = 0.11 \text{ wt}\%$). The inset shows images of the emission arising from the same PDI-EC mixture at both temperatures. b) TEM image of PDI@OC_SLPs (negative staining with uranyl acetate). c) Confocal fluorescence microscopy images of PDI@OC_SLPs at room temperature ($\lambda_{\text{exc}} = 458 \text{ nm}$, $\lambda_{\text{em}} > 475 \text{ nm}$). d) Photographs of a suspension of PDI@OC_SLPs in water at $20 \text{ }^\circ\text{C}$ and $70 \text{ }^\circ\text{C}$. e) Thermofluorochromic behavior of water suspensions of different PDI-loaded SLPs prepared. In all the images, the left, central and right cuvettes contain PDI@EC_SLPs, PDI@TC_SLPs and PDI@OC_SLPs, respectively. The images in a), d) and e) were taken in the dark and under illumination with a 365 nm UV lamp at different temperatures ($20 \text{ }^\circ\text{C}$, $40 \text{ }^\circ\text{C}$, $50 \text{ }^\circ\text{C}$, $55 \text{ }^\circ\text{C}$ or $70 \text{ }^\circ\text{C}$). For all the SLPs, $c_{\text{PDI}} = 0.22 \text{ wt}\%$.

Integration of thermofluorochromic nanoparticles into materials

Thermofluorochromic SLPs can be easily incorporated into macroscopic solid matrices (e.g., polymer films) to fabricate thermally-responsive luminescent nanocomposites. This is the case of poly(vinyl alcohol) films loaded with dispersed PDI@EC_SLPs ($0.8 \text{ wt}\%$), which

were prepared by simply drop-casting a colloidal suspension of the SLPs in aqueous PVA solution (**Figure 3a**). The presence of the embedded SLPs in the resulting materials was confirmed by different techniques. First, endothermic peaks at $T \sim 30\text{-}37^\circ\text{C}$ were found in the differential scanning calorimetry (DSC) thermogram of freshly prepared PDI@EC@PVA layers, which are characteristic of the melting process of micro- and nanostructures of EC⁴⁸ (**Figure 3b**). Second, scanning electron microscopy imaging of polymer film cross-sections showed the presence of nanometer-sized voids previously occupied by the dispersed EC particles (**Figure 3c**), which were selectively removed by prior treatment with CHCl_3 .

Interestingly, the obtained PDI@EC@PVA layers exhibited great optical transparency (**Figure 3a and 3c**), as demonstrated by the high light transmittance in the visible region ($\%T^{400\text{-}700\text{nm}} \sim 90\%$, **Figure S3a**) and the very low haze value measured (0.9 %). This was attributed to (a) the good dispersability of the nanometer-sized particles within the polymeric matrix that minimizes light scattering effects, and (b) the adequate refractive index matching between the SLPs and the surrounding PVA film. More importantly, the fabricated polymer layers fully reproduced the robust and reversible emission modulation previously observed upon thermal heating for PDI@EC_SLPs and bulk PDI-EC mixtures (**Figure 3c and Figure S3b**). In addition, rather high absolute fluorescence quantum yields could be measured for the two states of the PDI@EC_SLPs dispersed within the PVA matrix: (a) $\Phi_{\text{em}} = 0.77$ for the monomer emission obtained when heating above EC melting point, which is slightly lower than the values reported for typical PDI organic solutions^{44,45} probably due to self-absorption; (b) $\Phi_{\text{em}} = 0.36$ for the excimer-like emission at room temperature, a quite satisfactory value that we ascribed to limited self-quenching occurring upon aggregation thanks to the bulky side alkyl chains of the PDI dye. From all these results we could conclude that the surrounding polymer matrix maintains the discrete SLPs separated and the PDI molecules confined within the paraffin particles even after solid-liquid interconversion, thus ensuring the reversibility of the thermofluorochromic response of the nanocomposites. It is worth

mentioning that such behavior was achieved without the need of using PCM capsules coated with an impermeable shell, which allows maximizing the dye payload into the particles while ensuring that all emitter molecules lie embedded within the thermally-sensitive matrix.

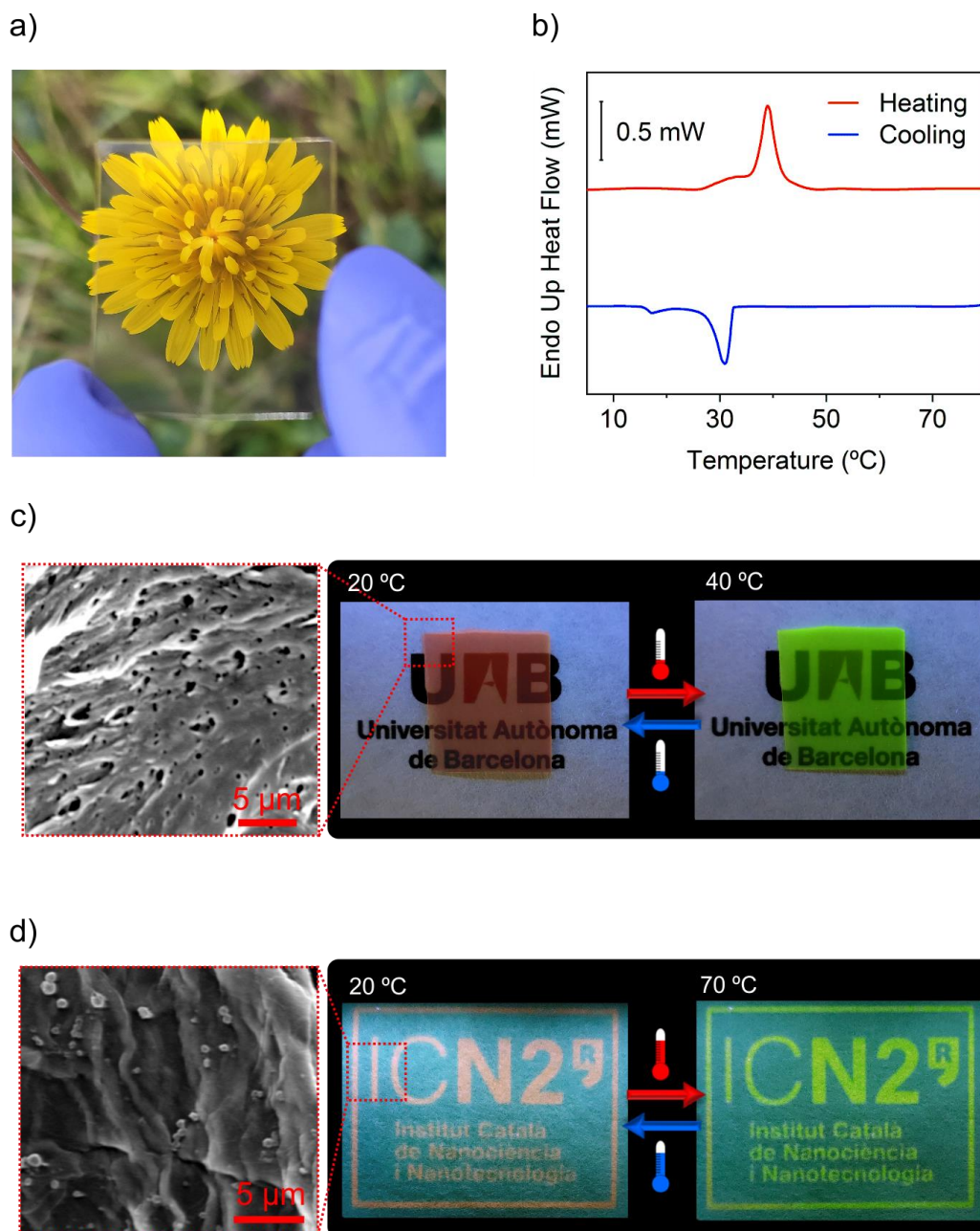


Figure 3. a) Photograph taken under ambient conditions of a transparent PDI@EC@PVA film (thickness $\sim 100 \mu\text{m}$). b) DSC thermogram of PDI@EC@PVA. c) Thermofluorochromic response of a transparent PDI@EC@PVA film when subjected to bulk heating. The inset shows a SEM image of a cross-section of the PDI@EC@PVA film after previous treatment with CHCl_3 for 2 hours. d) Thermofluorochromic response of a paper inkjet-printed with PDI@OC_SLPs. The inset shows a SEM image of a printed area of the paper. The emission arising from the samples in c) and d) was activated by illumination with a 365 nm UV lamp.

PDI-loaded SLPs could also be utilized for the formulation of water-based printable inks, thus removing the need for using organic solvents and coated cellulose substrates when

directly inkjet-printing bulk dye-PCM mixtures showing off-on thermofluorochromism.⁴⁰ Thus, we observed that by dispersing PDI-loaded SLPs (e.g., PDI@OC_SLPs, 1 wt%) in 20 wt% glycerol aqueous solutions, low-viscosity aqueous formulations were obtained that could be successfully inkjet-printed on regular paper. Glycerol is a commonly used additive for printable inks to control its viscosity and flow, which improves the resolution of the printed patterns. As shown in Figure 3d, well-resolved complex patterns could be deposited in this way, which retained the reversible and robust thermoresponsive fluorescent behavior of the printed SLPs. Interestingly, analysis of the printed motifs by electron microscopy revealed that most of the deposited dye-loaded SLPs lie well-separated onto the substrate (Figure 3d), which would open the door to print multiple particles with different behavior in the same area.

Multicolor-emissive thermofluorochromic materials

For the preparation of PCM-based multicolor thermofluorochromic materials using a single fluorophore, we integrated a mixture of PDI-loaded SLPs made from different types of PCMs into a single platform (e.g., a polymer layer), whose red-to-green color switching must occur at different temperatures to generate distinct combined emissions (**Figure 4a**). As an example, we prepared a PVA film containing equal amounts of PDI-loaded EC and OC SLPs (PDI@EC_{0.5}OC_{0.5}@PVA, $c_{\text{SLP}} = 1.6$ wt%). Analysis of the resulting polymer layer by DSC showed separate and defined thermal phase transitions that are compatible with the stepwise melting of these particles at their different T_m values ($T_m = 36.5$ °C and 61.3 °C⁴⁶; Figure S4). Consequently, the switching emission properties of both SLPs were maintained, and the expected red excimer-like and green monomeric emissions were measured at sufficiently low ($T = 20$ °C) and high ($T = 70$ °C) temperatures as to warrant that both types of SLPs were in the solid and liquid state, respectively. However, heating at intermediate temperatures between EC and OC melting points ($T = 40$ °C) led to a new yellow fluorescent state arising from the combination of the red emission from solid PDI@OC_SLPs and the green emission from melted PDI@EC_SLPs (Figure 4b). This was corroborated by the Commission

Internationale de l'Éclairage (CIE) 1931 chromaticity coordinates determined for the fluorescence spectrum registered at $T = 40\text{ °C}$ (0.44, 0.53), which fall within the color trajectory defined by the red (0.59, 0.39) and green (0.35, 0.57) emissions measured at $T = 20\text{ °C}$ and $T = 70\text{ °C}$, respectively (Figure S5a).

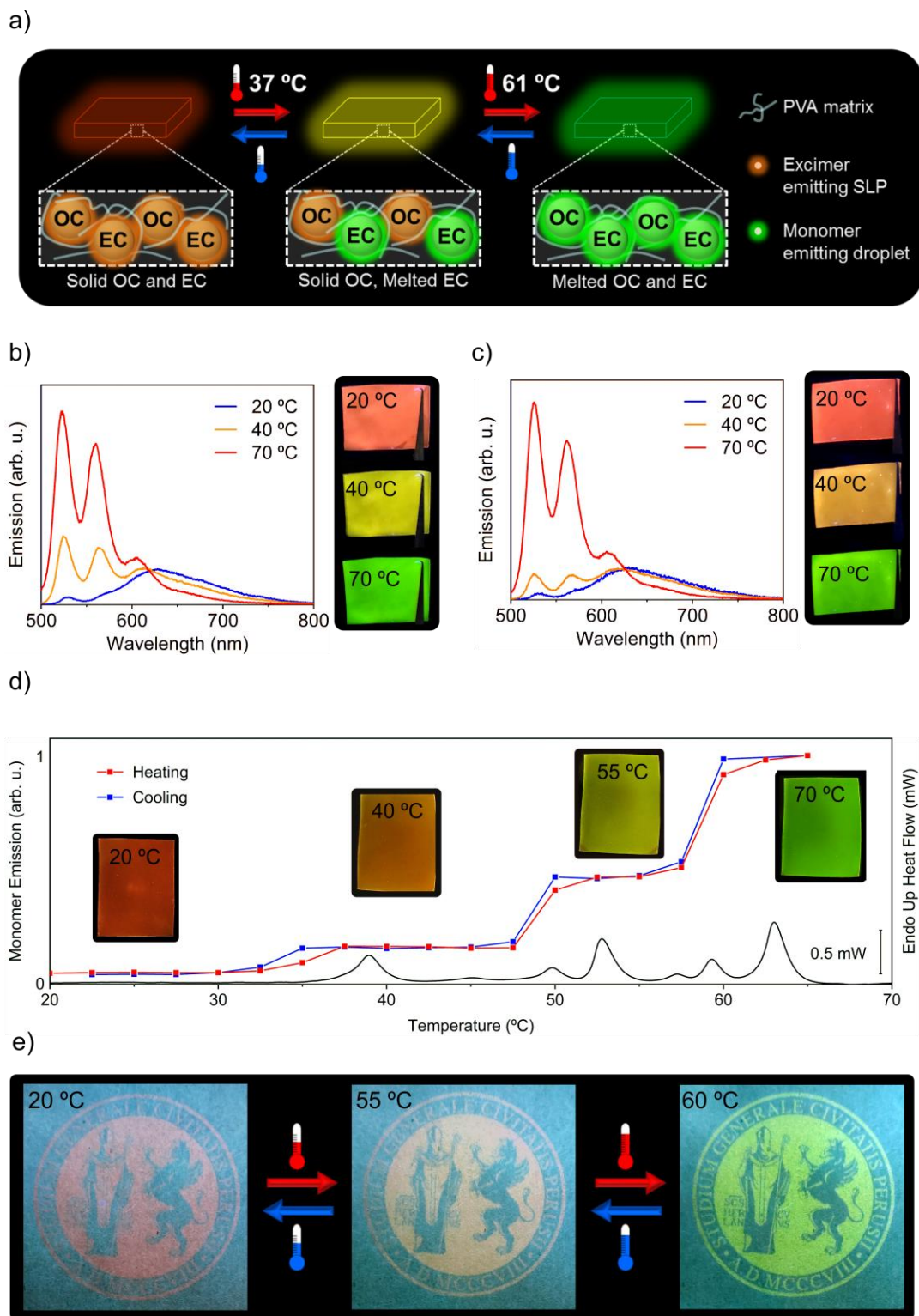


Figure 4. a) Strategy applied to obtain multicolor-emissive thermoresponsive materials, which consists in incorporating thermofluorochromic dye-loaded SLPs melting at different temperatures within the same film (e.g.,

PDI@EC_SLPs and PDI@OC_SLPs embedded in PVA films). b-c) Photographs and emission spectra ($\lambda_{\text{exc}} = 445 \text{ nm}$) of b) PDI@EC_{0.5}OC_{0.5}@PVA at 20 °C, 40 °C and 70 °C and c) PDI@EC_{0.2}OC_{0.8}@PVA at 20 °C, 40 °C and 70 °C. d) Thermal dependence of the monomeric emission at $\lambda_{\text{em}} = 445 \text{ nm}$ of PDI@EC_{0.2}TC_{0.3}OC_{0.5}@PVA, which is plotted together with the DSC thermogram of this polymer film. Photographs of the emission of the sample at 20 °C, 40 °C, 55 °C and 70 °C are shown as insets. e) Thermofluorochromic response of a paper inkjet-printed with a mixture of PDI@TC_SLPs and PDI@OC_SLPs. In the images in b-e) the emission from the films is activated by illumination with a 365 nm UV lamp.

The three-color thermofluorochromic response of polymeric films loaded with PDI@EC_SLPs and PDI@OC_SLPs could be easily fine-tuned by controlling the relative contribution of their different luminescence signals at intermediate temperatures - i.e., by modifying the concentration ratio of both families of SLPs in the material. For example, when a 1:4 PDI@EC_SLPs:PDI@OC_SLPs ratio was selected, a distinct thermal response was measured for the resulting PDI@EC_{0.2}OC_{0.8}@PVA layer ($c_{\text{SLP}} = 1 \text{ wt\%}$). Thus, while the low- T red and high- T green emissions remained nearly invariant, orange fluorescence was instead measured at $T = 40 \text{ °C}$ with CIE 1931 chromaticity coordinates (0.5, 0.46) (Figure 4c and Figure S5a).

In addition, the multicolor thermofluorochromic behavior of SLP-based composites could be further expanded by increasing the number of different nanoparticles within the material. This was proven by dispersing PDI-loaded SLPs made of EC ($T_{\text{m}} = 36.5 \text{ °C}^{46}$), TC ($T_{\text{m}} = 50.3 \text{ °C}^{46}$) and OC ($T_{\text{m}} = 61.3 \text{ °C}^{46}$) in a PVA film with a 2:3:5 concentration ratio (PDI@EC_{0.2}TC_{0.3}OC_{0.5}@PVA, $c_{\text{SLP}} = 1.6 \text{ wt\%}$) optimized to reach a four-state thermofluorochromic response. In this case, luminescence changed from red ($T = 20 \text{ °C}$) to green ($T = 70 \text{ °C}$) going through mixed orange ($T = 40 \text{ °C}$) and yellow ($T = 55 \text{ °C}$) colors by sequentially melting the three different types of nanostructured PCMs embedded (Figure 4d and Figure S5a-b). DSC measurements demonstrated that the variation of the contribution of PDI monomer emission to these spectra clearly correlates with the phase transitions registered for PDI@EC_{0.2}TC_{0.3}OC_{0.5}@PVA (Figure 4d). Importantly, the complex multicolor fluorescence response measured for this sample could be fully reverted upon subsequent

cooling, thus again proving that individual thermofluorochromic SLPs embedded within polymer matrices preserve their integrity.

Inkjet-printable aqueous-based colloidal suspensions containing different thermally-responsive PDI-loaded SLPs were also used to fabricate multicolor-switchable luminescent designs onto a bare substrate without any supporting solid polymer matrix. With this aim, an ink composed of both PDI@TC_SLPs and PDI@OC_SLPs was formulated and used to print at once a complex mark onto paper (Figure 4d). Clearly, three distinct red, orange and green luminescent signals could be retrieved for this image upon temperature variation as a result of the stepwise melting of its constituting SLPs, which were preserved after multiple cooling-heating cycles (Figure S6). Interestingly, such a robust and reproducible thermofluorochromic response could be accomplished despite simultaneously depositing different SLPs within the same locations of the printed motif with no separating polymer layer in between. Therefore, this does not only demonstrate that SLPs are initially well-dispersed and physically separated onto the cellulose substrate (see Figure 3d), but also that they do not merge nor lose their dye content upon repetitive solid-liquid interconversion.

Versatile applications of SLP-based multicolor thermofluorochromic materials

By facilitating their integration into multicomponent formulations and devices, the nanostructuring of PCM-based thermofluorochromic systems opens up a wider range of applications for these materials that encompasses a variety of fields. On the one hand, SLP-based polymer nanocomposites emerge as very promising components for the fabrication of color-tunable smart displays,^{7,49–52} especially for those applications that require high optical transparency, such as windows, and wearables head-up panels.⁴¹ However, in all the single-dye luminescent polymer layers described above, the different emission colors produced are constrained within the chromatic trajectory delimited by the emissions at the lowest and highest temperatures – i.e., from red excimer-like to green monomer emission. Therefore, to

fabricate true multicolor thermofluorochromic displays, other regions of the chromatic diagram must also be explored by adding additional fluorescent dyes. To do so, we chose 9,10-dicyanoanthracene (DCA, Figure S7a) as a supplementary emitter because its blue luminescence is complementary to the red and green fluorescence from PDI@SLPs (CIE 1931 chromatic coordinates (0.15, 0.09)). Actually, these three emission colors together define a chromatic triangle that encompasses most of the standard RGB (sRGB) color space generally used nowadays in monitors and printers (**Figure 5a** and Figure S7b). As a result, their combinations in different ratios must allow accomplishing the majority of the colors within the sRGB gamut, a feature that herein we aim to achieve using only two emitters in contrast to the usual approaches based on three dye cocktails.^{40,51}

With this goal in mind, transparent PVA films containing a dispersion of PDI-loaded SLPs and liquid DCA-loaded Miglyol[®] 812 nanodroplets (DCA@M812_NDs, Figure S8) were obtained. For this we adapted a methodology recently reported by us for the fabrication of photochromic films from oil nanoemulsions,⁵³ which herein required drop-casting a mixture of three different aqueous samples: a PVA solution in water (10 wt%), an aqueous colloidal suspension of PDI@EC_SLPs and PDI@OC_SLPs, and an oil-in-water nanoemulsion of a DCA solution in Miglyol[®] 812 ($c_{\text{DCA}} = 2.5 \text{ mM}$). Miglyol[®] 812, a mixture of decanoyl- and octanoyl glycerides distilled from coconut oil, was chosen as organic solvent for DCA because it solidifies at $T < 0 \text{ }^\circ\text{C}$ and boils at very high temperatures - i.e., it remains in the liquid state for all the thermal range of interest, thus preserving DCA blue monomeric emission.

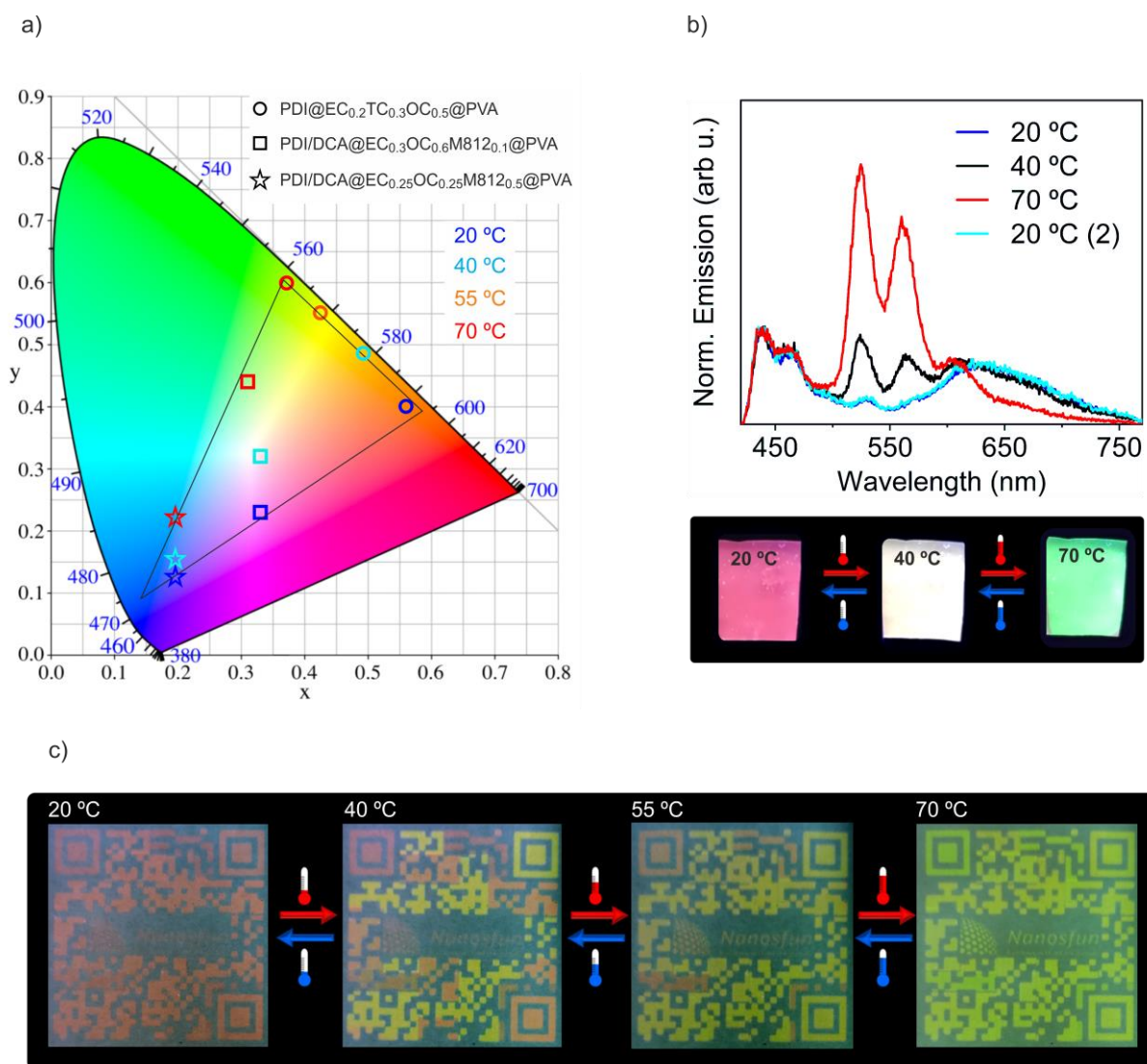


Figure 5. a) Temperature-dependent chromaticity coordinates of the emission of thermofluorochromic PVA nanocomposites prepared from PDI and DCA ($\lambda_{exc} = 405$ nm), which cover the chromatic color space delimited by black lines. For all the samples, measurements were registered at 20 °C, 40 °C and 70 °C, while additional data were recorded at 55 °C for PDI@EC_{0.2}TC_{0.3}OC_{0.5}@PVA. b) Emission spectra ($\lambda_{exc} = 405$ nm) and photographs of PDI/DCA@EC_{0.3}OC_{0.6}M812_{0.1}@PVA at 20 °C, 40 °C and 70 °C. The measurement at 20 °C (20 °C (2)) was repeated after a full cycle of heating to 70 °C and cooling down to room temperature. The fluorescence images of the films were taken upon illumination at 365 nm UV lamp. c) Thermofluorochromic QR code inkjet-printed onto paper using different inks based on separate PDI@EC_SLPs, PDI@TC_SLPs and PDI@OC_SLPs. All the images were taken under wide field illumination with a 365 nm UV lamp.

In the resulting films, different multicolor thermofluorochromic responses were obtained depending on the relative concentration of their embedded fluorophore nanostructures. To illustrate this principle, first films with a 3:6:1 ratio of PDI@EC_SLPs, PDI@OC_SLPs and DCA@M812_NDs, respectively, were designed to present white light luminescence ($c_{SLP} = 1.2$ wt%, $c_{ND} = 0.13$ wt%), a very much desired property for lighting.^{21,54,55} As designed, the temperature-dependence fluorescence of the resulting PDI/DCA@EC_{0.3}OC_{0.6}M812_{0.1}@PVA

films (Figure S8) showed a three-color reversible thermofluorochromic behavior: (a) pink at $T = 20\text{ }^{\circ}\text{C}$, with both SLPs in its solid state, (b) mint green at $T = 70\text{ }^{\circ}\text{C}$ with both SLPs melted, and (c) nearly pure white light luminescence with chromaticity coordinates (0.33, 0.32) at $T = 40\text{ }^{\circ}\text{C}$, thanks to the combination of the green fluorescence from melted PDI@EC_SLPs, the red emission from solid PDI@OC_SLPs and the blue luminescence from the liquid DCA@M812_NDs (Figure 5a-b). When another formulation with a 1:1:2 ratio of these nanostructures was used, the resulting PDI/DCA@EC_{0.25}OC_{0.25}M812_{0.5}@PVA film further shifted the color trajectory generated upon heating ($c_{\text{SLP}} = 0.5\text{ wt\%}$, $c_{\text{ND}} = 0.5\text{ wt\%}$), which in this case went from purple to cyan due to the increase in the content of the blue DCA-loaded nanodroplets (Figure 5a and Figure S9).

Another potential application of PCM-based multicolor thermofluorochromic materials is high level information encoding for anti-counterfeiting, which does not only benefit from their complex and highly tunable thermally-induced emissive responses, but also from the viability as inkjet-printable mixtures. To test this concept, we performed simultaneous printing of colloidal inks made from three PDI-loaded nanoparticles, namely PDI@EC_SLPs, PDI@TC_SLPs or PDI@OC_SLPs. As an example, we used these inks to print the distinct pixels of a QR code, for which four different thermofluorochromic responses were registered (Figure 5c). Thus, pure red emission was observed at room temperature where all the printed SLPs remained in the solid state, whereas sequential transformation towards green fluorescence was observed by heating at 40, 55 and 70 °C for selectively melting the EC-, TC- and OC-containing pixels, respectively. In this way, fourth-level data encryption and decryption were accomplished by means of SLP-based security inks using a single emitter, which could be even further improved by introducing other PCMs and/or dyes. This therefore demonstrates that multicolor thermofluorochromic materials based on nanostructured PCM-dye mixtures allow for the multilevel detection of security labels, the most advanced type of luminescent anti-counterfeiting mode.^{8,9,16–18,43}

Local NIR-induced photothermofluorochromism

To add further functionality to the multicolor SLP-based thermofluorochromic materials developed herein, we took advantage of our previous demonstration³⁵ that the thermally-induced emission response of bulk dye-PCM mixtures can also be phototriggered by the heat generated by plasmonic gold nanoshells (AuNSs)⁵⁶⁻⁵⁸ under near-infrared (NIR) irradiation. In light of this precedent, we decided to prepare PVA nanocomposites bearing both PDI@EC_SLPs and 80-nm in diameter AuNSs (0.02 wt%, Figure S10), which under NIR illumination should be capable of photothermally melt the neighboring PCM nanostructures to elicit light-induced fluorescence modulation. The resulting PVA layers preserved high optical transparency despite the presence of additional dispersed nanostructures ($\%T^{400-700\text{nm}} \sim 80\%$, haze = 0.9%, Figure S11) and, more importantly, they exhibited thermofluorochromic responses that could be triggered both under bulk thermal heating or locally from afar using point illumination with a collimated NIR laser (**Figure 6a**). In addition, the photoinduced emission changes were found to be fast and entirely reproducible and robust if consecutive cycles of photothermal heating and cooling were applied (Figure S12).

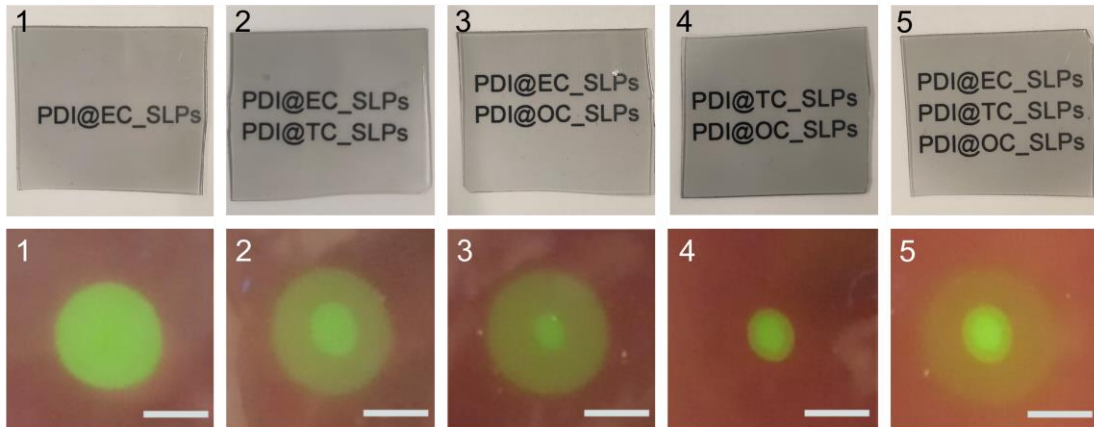
To expand the photothermofluorochromic behavior to multicolor emissive nanocomposites, we prepared a set of transparent PVA films loaded with AuNSs and binary (PDI@EC_SLPs and PDI@TC_SLPs; PDI@EC_SLPs and PDI@OC_SLPs; PDI@TC_SLPs and PDI@OC_SLPs) and ternary (PDI@EC_SLPs, PDI@TC_SLPs and PDI@OC_SLPs) mixtures of PDI-based SLPs. When inspected by naked eye at room temperature under ambient light or in the dark upon UV irradiation, all these films looked similar between them and equivalent to the sample loaded with only PDI@EC_SLPs – i.e., optically transparent and red emitting (Figure 6b and Figure S13a). On the other hand, irradiation with a NIR laser beam ($\lambda_{\text{exc}} = 830 \text{ nm}$, 1300 mW cm^{-2} , 2.5 mm in diameter spot) developed distinct concentric fluorescent patterns. These macroscopically tangible signals and contrasts for each formulation arose as a result of three combined and controlled effects: (a) the different T_m

values of the SLPs used; (b) the photothermal heating of the substrate induced by plasmonic excitation of AuNSs, which generates a temperature gradient as moving away from the NIR-illuminated spot (Figure 6c); (c) the different type and amount of molten PDI-loaded SLPs under such temperature gradient, which yields different emission colors ranging from pure green monomer fluorescence (if all SLPs are melted) to distinct red-green luminescence mixtures (if some of them remain in the solid state). Therefore, several thermofluorochromic patterns could be generated from apparently similar polymer layers that univocally correlated with the composition of the SLP-loaded polymer nanocomposites. These properties, together with their simplicity, low cost, reusability, optical transparency and mechanical flexibility, make SLP-loaded polymer nanocomposites very attractive materials for the fabrication of cryptographic labels for security protection.^{8,9,16-18,43}

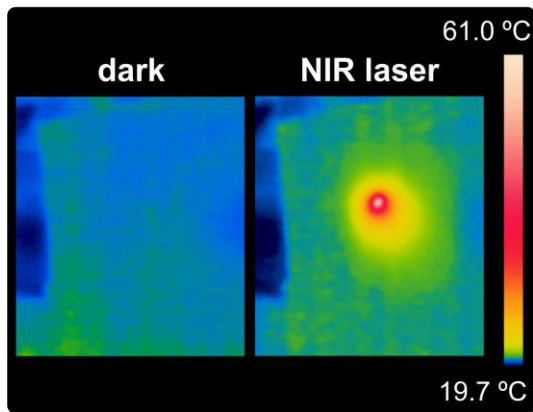
a)



b)



c)



d)

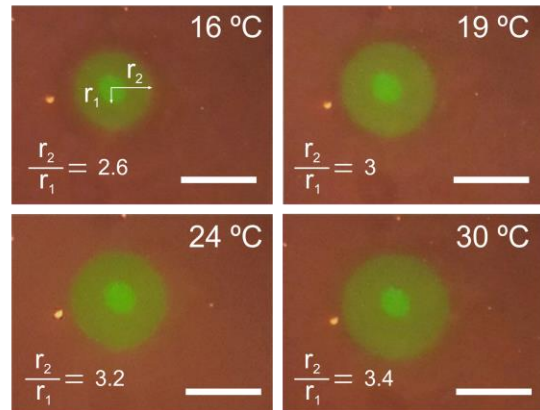


Figure 6. a) Images of the thermofluorochromic behavior of a transparent PVA film loaded with PDI@EC_SLPs and AuNSs when subjected to bulk heating or local photothermal heating with a NIR laser ($\lambda_{\text{exc}} = 830 \text{ nm}$, 1300 mW cm^{-2}). b) Photographs of different PVA films loaded with PDI-based SLPs and AuNSs (0.02 wt%) under ambient light (top), and UV excitation ($\lambda_{\text{exc}} = 365 \text{ nm}$) together with NIR-point illumination ($\lambda_{\text{exc}} = 830 \text{ nm}$, 1300 mW cm^{-2} , 2.5 mm in diameter spot) in the dark (bottom). All the measurements were conducted at 21.5 °C. c) Steady state temperature profile generated on a PDI@EC_SLPs@PVA film loaded with AuNSs (0.02 wt%) under continuous NIR-point illumination ($\lambda_{\text{exc}} = 830 \text{ nm}$, 1300 mW cm^{-2} , 2.5 mm in diameter spot). d) Photographs of the NIR-induced fluorescent patterns created in a PVA film loaded with AuNSs (0.034 wt%) and a 1:1 mixture of PDI@EC_SLPs and PDI@OC_SLPs when varying the external temperature from 16 °C to 30 °C. All the images were taken under wide field illumination with a 365 nm UV lamp and point irradiation with a NIR laser ($\lambda_{\text{exc}} = 830 \text{ nm}$, 1300 mW cm^{-2} , 2.5 mm in diameter spot).

Worth to mention, the temperature gradient created around the irradiated regions of the photothermally-responsive polymer layers could be fine-tuned with two additional parameters. First, varying the NIR excitation intensity should lead to differential photothermal heating, thus resulting in diverse luminescent patterned signals for the same sample composition. This was demonstrated for a binary mixture of PDI@EC_SLPs and PDI@OC_SLPs embedded in PVA, where different size ratios between the inner green and external yellow fluorescent circles were measured when tuning the NIR illumination power (Figure S13b). Importantly, such an abundance of distinct quantifiable optical responses is a requirement to achieve multilevel information encoding and decoding in stimuli-responsive materials, an especially demanded feature for high security marking.^{8,9,16–18,43} The second parameter is the external temperature, as it may alter the extent of the NIR-induced thermal gradient created onto the substrate, thereby affecting the thermofluorochromic responses. In particular, a gradual variation of the size ratio of the concentric fluorescent signals (r_2/r_1 , where r_1 and r_2 are the radii of the inner and outer concentric circles, respectively) was measured maintaining constant the NIR irradiation power but modifying the external temperature (Figure 6d). Consequently, this opens the door to apply SLP-loaded polymer nanocomposites as variable thermal fluorescent sensors,³ a quite remarkable feature as they are composed of PCM-based particles showing stepwise emission switching at a single temperature.

Conclusions

In this work we introduced a novel strategy for the fabrication of multicolor thermofluorochromic systems, which capitalizes on the well-known capacity of phase change materials to induce a sharp and reversible change of dyes emission upon solid-liquid transition. We herein expanded this concept to the realization of multiple color fluorescence switching in a simple, universal, cost-effective and versatile manner, which is based on two main findings. First, we demonstrated that PCM-based thermofluorochromism can be transferred to the

nanoscale by preparing dye-loaded solid lipid nanoparticles, which can be easily integrated into composite materials (e.g., transparent polymer films) and used for the preparation of colloidal inks (e.g., for inkjet printing). Second, we showed that multicolor thermofluorochromism can be obtained by combining several different of these nanoparticles in a single platform, even if all of them contain the same class of fluorophore. Because of the simplicity and variability of the composition of thermofluorochromic SLPs, their facile and adaptable processability, and the feasibility to drive their operation photothermally under NIR irradiation, a variety of thermoresponsive multicolor-emissive systems can be prepared in this way, which we proved that can be used for a wide range of applications such as white light generation in smart luminescent displays, multithreshold thermal sensing and high-security anti-counterfeiting.

Author Contributions

J. H. and C. R. conceived the idea, and designed and supervised the research. J. R. O. and C. R. designed and performed the experiments, and analyzed the data. All authors discussed the results, and wrote and revised the manuscript.

Conflict of Interest

The authors declare no conflict of interest.

Supporting Information

Additional data on the materials prepared and their optical properties.

Acknowledgements

This work was supported by MINECO/FEDER (CTQ2015-65439-R and RTI2018-098027-B-C21 projects) and Generalitat de Catalunya (2017 SGR00465 project). J. R. O. thanks the Generalitat de Catalunya (AGAUR) for his predoctoral FI fellowship. ICN2 acknowledges support from the Severo Ochoa programme (MINECO, SEV-2017-0706) and the CERCA programme (Generalitat de Catalunya). L. L. is grateful to Ministero dell'Istruzione, dell'Università e della Ricerca (MIUR) for the support through the program "Dipartimenti di Eccellenza 2018-2022" (grant AMIS) and acknowledges CSGI (Consorzio Interuniversitario per lo Sviluppo dei Sistemi a Grande Interfase, Research Center for Colloid and Surface Science) for the support. We acknowledge the Research Support Division - Instrumentation Unit of ICN2 for the help in the instrumentation design.

References

- 1 X. Wang, O. S. Wolfbeis and R. J. Meier, *Chem. Soc. Rev.*, 2013, **42**, 7834.
- 2 A. Julià López, D. Ruiz-Molina, K. Landfester, M. B. Bannwarth and C. Roscini, *Adv. Funct. Mater.*, 2018, **28**, 1–7.
- 3 M. M. A. Mazza and F. M. Raymo, *J. Mater. Chem. C*, 2019, **7**, 5333–5342.
- 4 J. Zhou, B. del Rosal, D. Jaque, S. Uchiyama and D. Jin, *Nat. Methods*, 2020, **17**, 967–980.
- 5 A. Kishimura, T. Yamashita, K. Yamaguchi and T. Aida, *Nat. Mater.*, 2005, **4**, 546–549.
- 6 S. Hirata, K.-S. Lee and T. Watanabe, *Adv. Funct. Mater.*, 2008, **18**, 2869–2879.
- 7 K. Ogasawara, K. Nakamura and N. Kobayashi, *J. Mater. Chem. C*, 2016, **4**, 4805–4813.
- 8 W. Ren, G. Lin, C. Clarke, J. Zhou and D. Jin, *Adv. Mater.*, 2020, **32**, 1901430.
- 9 A. Abdollahi, H. Roghani-Mamaqani, B. Razavi and M. Salami-Kalajahi, *ACS Nano*,

- 2020, **14**, 14417–14492.
- 10 B. R. Crenshaw and C. Weder, *Chem. Mater.*, 2003, **15**, 4717–4724.
 - 11 A. Pucci, F. Di Cuia, F. Signori and G. Ruggeri, *J. Mater. Chem.*, 2007, **17**, 783–790.
 - 12 L. H. Fischer, G. S. Harms and O. S. Wolfbeis, *Angew. Chemie Int. Ed.*, 2011, **50**, 4546–4551.
 - 13 J. Feng, K. Tian, D. Hu, S. Wang, S. Li, Y. Zeng, Y. Li and G. Yang, *Angew. Chemie Int. Ed.*, 2011, **50**, 8072–8076.
 - 14 J. Feng, L. Xiong, S. Wang, S. Li, Y. Li and G. Yang, *Adv. Funct. Mater.*, 2013, **23**, 340–345.
 - 15 D. Ruiz, B. del Rosal, M. Acebrón, C. Palencia, C. Sun, J. Cabanillas-González, M. López-Haro, A. B. Hungría, D. Jaque and B. H. Juarez, *Adv. Funct. Mater.*, 2017, **27**, 1604629.
 - 16 R. Liao, S. Gu, X. Wang, X. Zhang, X. Xie, H. Sun and W. Huang, *J. Mater. Chem. C*, 2020, **8**, 8430–8439.
 - 17 S. Liu, Y. Ma, S. Liu, K. Chen, W. Huang and Q. Zhao, *J. Mater. Chem. C*, 2020, **8**, 10798–10804.
 - 18 X. Yu, H. Zhang and J. Yu, *Aggregate*, 2021, **2**, 20–34.
 - 19 Z. Xie, C. Chen, S. Xu, J. Li, Y. Zhang, S. Liu, J. Xu and Z. Chi, *Angew. Chemie Int. Ed.*, 2015, **54**, 7181–7184.
 - 20 D. Li, W. Hu, J. Wang, Q. Zhang, X.-M. Cao, X. Ma and H. Tian, *Chem. Sci.*, 2018, **9**, 5709–5715.
 - 21 N. A. Vázquez-Mera, J. R. Otaegui, R. S. Sánchez, G. Prats, G. Guirado, D. Ruiz-Molina, C. Roscini and J. Hernando, *ACS Appl. Mater. Interfaces*, 2019, **11**, 17751–17758.
 - 22 A. Seeboth, D. Löttsch, R. Ruhmann and O. Muehling, *Chem. Rev.*, 2014, **114**, 3037–3068.

- 23 K. Totani, Y. Okada, S. Hirata, M. Vacha and T. Watanabe, *Adv. Opt. Mater.*, 2013, **1**, 283–288.
- 24 J. Wang, N. Wang, G. Wu, S. Wang and X. Li, *Angew. Chemie Int. Ed.*, 2019, **58**, 3082–3086.
- 25 Y. Cao, J. K. Nagle, M. O. Wolf and B. O. Patrick, *J. Am. Chem. Soc.*, 2015, **137**, 4888–4891.
- 26 L. Liu, X. Wang, N. Wang, T. Peng and S. Wang, *Angew. Chemie Int. Ed.*, 2017, **56**, 9160–9164.
- 27 C. Li, Y. Zhang, J. Hu, J. Cheng and S. Liu, *Angew. Chemie Int. Ed.*, 2010, **49**, 5120–5124.
- 28 V. K. Praveen, S. J. George, R. Varghese, C. Vijayakumar and A. Ajayaghosh, *J. Am. Chem. Soc.*, 2006, **128**, 7542–7550.
- 29 J. Liu, Y. Zhang, C. Zhang, P. Zhang, R. Zeng, J. Cui and J. Chen, *Mater. Adv.*, 2020, **1**, 1330–1336.
- 30 M. D. Johnstone, C.-W. Hsu, N. Hochbaum, J. Andréasson and H. Sundén, *Chem. Commun.*, 2020, **56**, 988–991.
- 31 J. A. H. P. Sol, V. Dehm, R. Hecht, F. Würthner, A. P. H. J. Schenning and M. G. Debije, *Angew. Chemie Int. Ed.*, 2018, **57**, 1030–1033.
- 32 Z.-Q. Yu, X. Li, W. Wan, X.-S. Li, K. Fu, Y. Wu and A. D. Q. Li, *Chem. Sci.*, 2021, **12**, 3146–3151.
- 33 G. Massaro, J. Hernando, D. Ruiz-Molina, C. Roscini and L. Latterini, *Chem. Mater.*, 2016, **28**, 738–745.
- 34 G. Massaro, G. Zampini, D. Ruiz-Molina, J. Hernando, C. Roscini and L. Latterini, *J. Phys. Chem. C*, 2019, **123**, 4632–4637.
- 35 J. R. Otaegui, P. Rubirola, D. Ruiz-Molina, J. Hernando and C. Roscini, *Adv. Opt. Mater.*, 2020, **8**, 2001063.

- 36 Y. J. Jin, R. Dogra, I. W. Cheong and G. Kwak, *ACS Appl. Mater. Interfaces*, 2015, **7**, 14485–14492.
- 37 J. Du, L. Sheng, Q. Chen, Y. Xu, W. Li, X. Wang, M. Li and S. X. Zhang, *Mater. Horizons*, 2019, **6**, 1654–1662.
- 38 T. Qin, J. Du, C. Wang, L. Sheng and S. X.-A. Zhang, *J. Mater. Chem. C*, 2019, **7**, 9149–9153.
- 39 Y. J. Jin, Y. G. Choi, H. Park and G. Kwak, *J. Mol. Liq.*, 2018, **265**, 260–268.
- 40 J. Du, L. Sheng, Y. Xu, Q. Chen, C. Gu, M. Li and S. X. Zhang, *Adv. Mater.*, 2021, **33**, 2008055.
- 41 G. Huseynova, J. Lee, Y. H. Kim and J. Lee, *Adv. Opt. Mater.*, 2021, 2002040.
- 42 J. A. H. P. Sol, G. H. Timmermans, A. J. van Breugel, A. P. H. J. Schenning and M. G. Debije, *Adv. Energy Mater.*, 2018, **8**, 1702922.
- 43 W. Yao, Q. Tian and W. Wu, *Adv. Opt. Mater.*, 2019, **7**, 1801171.
- 44 F. Würthner, *Chem. Commun.*, 2004, 1564–1579.
- 45 L. Parejo, M. Chaari, S. Santiago, G. Guirado, F. Teixidor, R. Núñez and J. Hernando, *Chem. – A Eur. J.*, 2021, **27**, 270–280.
- 46 D. R. Lide, *CRC Handbook of Chemistry and Physics*, CRC Press, Boca Raton, FL, 2016.
- 47 W. Mehnert and K. Mäder, *Adv. Drug Deliv. Rev.*, 2012, **64**, 83–101.
- 48 C. Alkan, A. Sarı and A. Karaipekli, *Energy Convers. Manag.*, 2011, **52**, 687–692.
- 49 W. Zhang, Y. Zhang, F. Xie, X. Jin, J. Li, G. Yang, C. Gu, Y. Wang and S. X. Zhang, *Adv. Mater.*, 2020, **32**, 2003121.
- 50 P. Audebert and F. Miomandre, *Chem. Sci.*, 2013, **4**, 575–584.
- 51 G. Naren, C.-W. Hsu, S. Li, M. Morimoto, S. Tang, J. Hernando, G. Guirado, M. Irie, F. M. Raymo, H. Sundén and J. Andréasson, *Nat. Commun.*, 2019, **10**, 3996.
- 52 L. Hou, X. Zhang, G. F. Cotella, G. Carnicella, M. Herder, B. M. Schmidt, M. Pätzelt, S.

- Hecht, F. Cacialli and P. Samorì, *Nat. Nanotechnol.*, 2019, **14**, 347–353.
- 53 H. Torres-Pierna, D. Ruiz-Molina and C. Roscini, *Mater. Horizons*, 2020, **7**, 2749–2759.
- 54 B. W. D’Andrade and S. R. Forrest, *Adv. Mater.*, 2004, **16**, 1585–1595.
- 55 H. Wu, L. Ying, W. Yang and Y. Cao, *Chem. Soc. Rev.*, 2009, **38**, 3391.
- 56 L. Latterini and L. Tarpani, in *Bio- and Bioinspired Nanomaterials*, Wiley-VCH Verlag GmbH & Co. KGaA, Weinheim, Germany, 2014, pp. 173–200.
- 57 L. Latterini and L. Tarpani, *J. Phys. Chem. C*, 2011, **115**, 21098–21104.
- 58 B. Storti, F. Elisei, S. Abbruzzetti, C. Viappiani and L. Latterini, *J. Phys. Chem. C*, 2009, **113**, 7516–7521.